Revision of Paleogene plate motions in the Pacific and implications for the Hawaiian-Emperor bend

Nicky M. Wright, R. Dietmar Müller, Maria Seton, and Simon E. Williams
EarthByte Group, School of Geosciences, University of Sydney, Sydney, NSW 2006, Australia

ABSTRACT

Understanding the relative motion between the Pacific plate and its neighboring plates in the Paleogene has important consequences for deciphering the relationship between absolute and relative plate motions in the Pacific Ocean basin, the history of circum-Pacific subduction, and the cause of the Hawaiian-Emperor bend (HEB). We quantitatively model the Farallon/Vancouver-Pacific-Antarctic seafloor spreading history from 67 to 33 Ma based on a comprehensive synthesis of magnetic anomaly and fracture identifications. We find a well-constrained increase from 75 ± 5 mm/yr to 101 ± 5 mm/yr in Pacific-Farallon full spreading rates between 57.6 Ma and 55.9 Ma, followed by a stepwise increase to 182 ± 2 mm/yr from 49.7 to 40.1 Ma. The increases in Pacific-Farallon spreading rates are not accompanied by any statistically significant change in spreading direction. The 57.6–55.9 Ma surge of Pacific-Farallon spreading reflects an eastward acceleration in Farallon plate motion, as it precedes west Pacific subduction initiation and is not associated with any significant change in Pacific-Antarctic spreading. We interpret the increase in Pacific-Farallon spreading rates after ca. 50 Ma as a consequence of further acceleration in Farallon plate motion. We find no indication of a major change in Pacific plate absolute motion at this time. Our model suggests that changes in relative motion direction between the Pacific and Farallon and Pacific and Antarctic plates were insignificant around the formation time of the HEB (ca. 47.5 Ma), and the bend is largely a consequence of Hawaiian hotspot motion, which ceased rapid motion after 47 Ma.

INTRODUCTION

The Hawaiian-Emperor bend (HEB) was traditionally interpreted as a relict of a large change in absolute plate motion in the context of the fixed hotspot hypothesis, but this interpretation has been questioned (e.g., Norton, 1995; Chandler et al., 2012; Tarduno, 2007). Recent dates of the age of the HEB indicate that the arcuate region of the Hawaiian-Emperor Seamount Chain (e.g., Daikakuji and Yuryaku seamounts; Fig. 1A) formed at ca. 47.5 Ma (O'Connor et al., 2013) and initial stages of the bend formed at ca. 50 Ma (near the Kimmei seamount) (O'Connor et al., 2013; Sharp and Clague, 2006). This age is ~3 m.y. younger than the onset of the regional Eocene plate reorganization (Whittaker et al., 2007). Analyses of paleolatitudes from paleomagnetic versus hotspot track data (Tarduno et al., 2003), mantle flow models (e.g., Steinberger et al., 2004), the relative motion between the Hawaii and Louisville hotspots (O'Connor et al., 2013), and predictions of the Hawaiian-Emperor Seamount Chain from plate circuits (e.g., Cande et al., 1995; Doubrovine and Tarduno, 2008) all point to the time dependence of Hawaiian plume motion as a major contributing factor to the HEB. Tarduno et al. (2009) explicitly suggested that the HEB may reflect mantle plume dynamics in the absence of a major change in plate motion. However, Koivisto et al. (2014) proposed that paleolatitude differences of the Emperor seamounts can be explained by true polar wander, although this explanation was questioned by analysis of paleomagnetic data (Tarduno, 2007). Koivisto et al. (2014) suggested that the HEB can be explained by a plate reorganization, an idea reinforced by Barckhausen et al. (2013), who concluded the HEB is coincident with a major acceleration in Pacific-Farallon spreading rates. Most published models for relative plate motions in the Pacific Ocean basin lack uncertainties, and studies that provide uncertainties (e.g., Rowan and Rowley, 2014) rely on long stages (e.g., ~7 m.y.), making it difficult to assess the significance and timing of any given tectonic event. Here we present revised relative plate motions with uncertainties for the Pacific Ocean basin during the Paleogene. Using a quantitative approach, we combine and analyze an unprecedented number of magnetic anomaly and fracture zone identifications from the eastern and southern Pacific Ocean basin spreading centers, i.e., the Pacific-Farallon/Vancouver ridge and the Pacific-Antarctic Ridge (Fig. 1). This four-plate analysis allows us to relate relative motion between plates to absolute plate motions (i.e., plate motion with respect to the underlying mantle), considering that the two are tightly connected, and test the plate reorganization hypothesis for the formation of the HEB.

METHODOLOGY

Rotation poles were obtained using the method of Royer and Chang (1991). Magnetic anomaly identifications are based on a compilation (by Seton et al., 2014), which uses a self-consistent set of magnetic identifications with identical attributes (i.e., chron and anomaly end) (Fig. 1). Ages attributed to chrons are based on the time scale of Cande and Kent (1995). Fracture zone interpretations are based on Matthews et al. (2011). Assigned uncertainties of the magnetic lineations are 6.9 km (Pacific-Antarctic) and 7.8 km (Pacific-Farallon/Vancouver), and fracture zones are 5 km (Müller et al., 1991).

We derive finite rotations for the Pacific-Antarctic seafloor spreading history between chron 30o (67.6 Ma) and chron 21o (47.9 Ma) and rely on well-constrained published rotations (Croon et al., 2008) for more recent times. In addition, we compute half-stage rotations for the Pacific-Farallon and Pacific-Vancouver seafloor spreading histories between chron 31y (67.7 Ma) and chron 13y (33.1 Ma), as finite rotations cannot be directly calculated due to subduction of the former Farallon and Vancouver plates. We rely on magnetic identifications north of the Pioneer Fracture Zone (Fig. 1B) for Pacific-Vancouver spreading, and south of the Murray Fracture Zone (Fig. 1C) for Pacific-Farallon spreading, based on the location of the former Vancouver plate boundary (Atwater, 1989). The Pacific-Farallon/Vancouver half-stage rotation poles were transformed into stage poles and finite Euler poles based on assumed symmetric spreading and standard statistical techniques. All stage spreading rates and directions represent the mean for a given tectonic stage.

RESULTS

Our results produce well-constrained Pacific-Farallon/Vancouver half-stage rotations, reflecting the abundant magnetic identifications and well-defined fracture zones on the Pacific plate (Fig. 1). We express all spreading rates derived from half-stage rotations as full spreading rates to enable a straightforward comparison with spreading rates derived from finite reconstruction poles (e.g., Pacific-Antarctic rotations). Our Pacific-Farallon full spreading rates initially increased from 75 ± 5 mm/yr at 57.6 Ma (chron 26y) to 101 ± 5 mm/yr at 55.9 Ma (chron 25y) (Fig. 2). This initial increase at 55.9 Ma was followed by a further stepwise increase in spreading rates, from 118 ± 6 mm/yr to 182 ± 2 mm/yr, between 49.7 Ma (chron 22o) and 40.1 Ma (chron 18n.2o) (Fig. 2). The increases in Pacific-Farallon spreading rates were not accompanied by a statistically significant change in spreading direction (Fig. 2). These results are not strongly dependent on the time scale used: based on the time scale of Ogg (2012), we observe a significant increase in spreading rate at ca. 57 Ma from 68 ± 4 mm/yr to 78 ± 5 mm/yr, followed by an increase at ca. 49 Ma from 77 ± 2 mm/yr to 106

GEOLOGY Data Repository item 2015156 | doi:10.1130/G36303.1

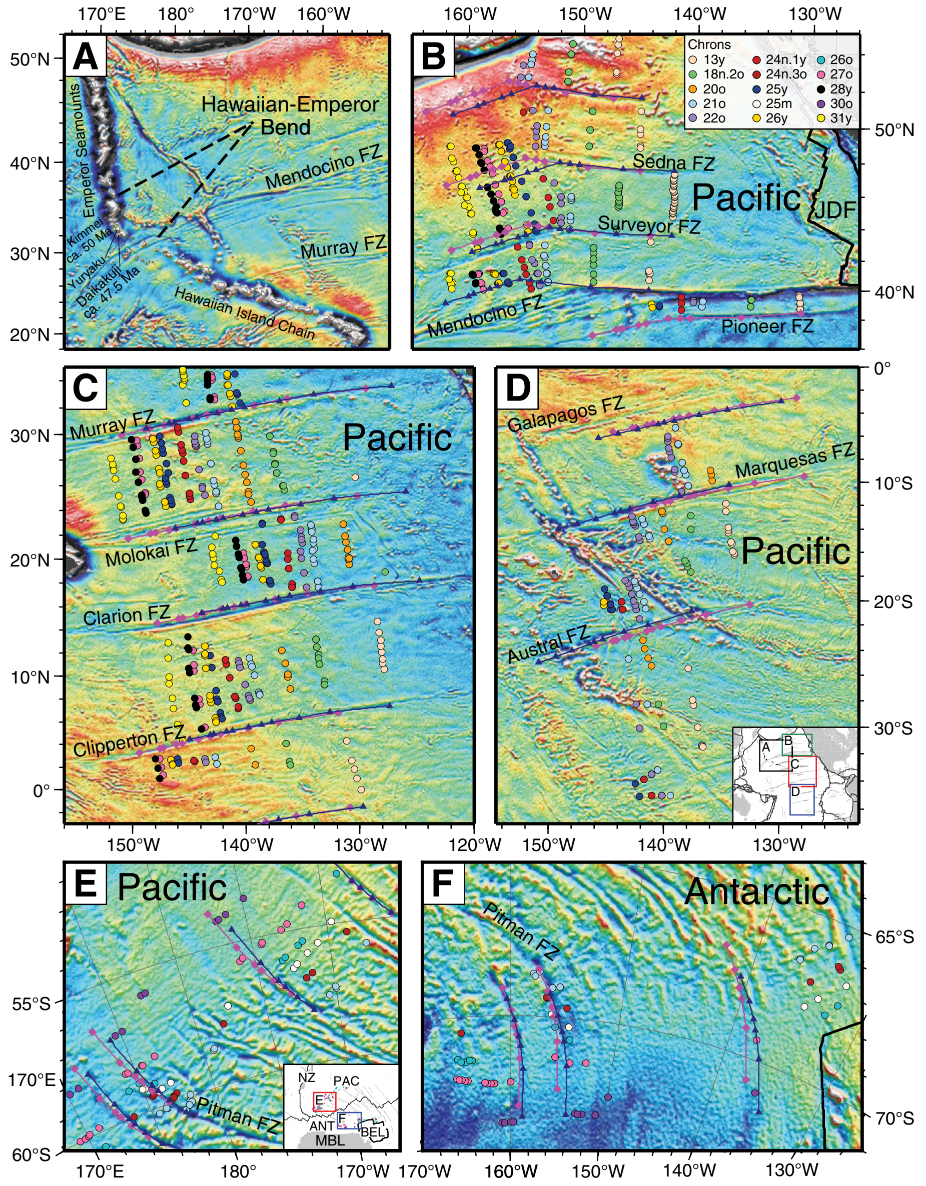

Figure 1. Overview of the Pacific Ocean basin. A: Hawaiian-Emperor Seamount Chain, including key seamounts identified by O'Connor et al. (2013) and Sharp and Clague (2006). Note that the age for Kimmei is based on interpolation. Flowlines, magnetic identifications used in our analysis, and fracture zones (FZ; observed in gravity anomaly), are shown in the northeastern Pacific (B) (Pacific-Vancouver/Farallon). C: The central-North Pacific (Pacific-Farallon). D: The South Pacific (Pacific-Farallon). E: The Pacific plate (Pacific-Antarctic). F: The Antarctic plate (Pacific-Antarctic). Flowlines and symbols corresponding with magnetic identification times are plotted at the east (dark blue, triangles) and west (magenta, diamonds) ridge-transform intersections. JDF—Juan de Fuca plate; NZ—New Zealand; MBL—Marie Byrd Land (Antarctica); PAC—Pacific plate; ANT—Antarctic plate; BEL—Bellingshausen plate.

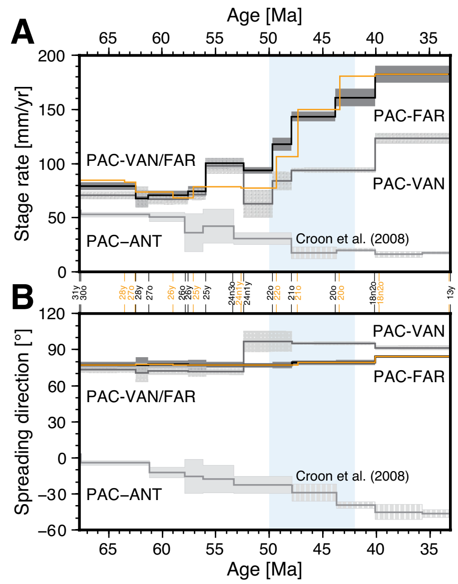

Figure 2. A: Full spreading rate and 95% uncertainty. B: Spreading direction and 95% uncertainty. Spreading systems include Pacific-Farallon (PAC-FAR) (dark gray) (also in Ogg, 2012; in orange), Pacific-Vancouver (PAC-VAN; dotted light gray), and Pacific-Antarctic (PAC-ANT; light gray). Chrons in the time scales of Cande and Kent (1995; black) and Ogg (2012; orange) are shown. Spreading parameters and uncertainties prior to 40.1 Ma are from Croon et al. (2008) (vertical lines). Prior to 52.4 Ma, Vancouver was part of the Farallon plate (VAN/FAR). Rates were calculated on the Molokai Fracture Zone (FZ) (PAC-FAR), Mendocino FZ (PAC-VAN), and Pitman FZ (PAC-ANT). The Hawaiian-Emperor bend (HEB) formed between ca. 50 Ma and ca. 42 Ma; the arcuate region formed at 47.5 Ma (shaded background).

± 5 mm/yr (Fig. 2). We also find similar increases in spreading rate when we consider asymmetric spreading (Fig. DR2 in the GSA Data Repository[1]). The initial increase in spreading precedes the previously suggested ages of spreading increase, ca. 53 Ma (chron 24; Rowan and Rowley, 2014) and ca. 47 Ma (chron 21; Barckhausen et al., 2013; Cande and Haxby, 1991). We find a similar trend in Pacific-Vancouver spreading rates; however, we observe a large change in spreading direction at 52.4 Ma (chron 24n.1y) (Fig. 2). This reflects the break-up of the Farallon plate to form the Vancouver plate, and is well supported by the clockwise direction implied by fracture zone trends, e.g., the Mendocino Fracture Zone (Fig. 1B). Our model produces well-constrained Pacific-Antarctic finite rotations, and finds a significant decrease in Pacific-Antarctic spreading rate and direction at ca. 53 Ma (42 ± 17 mm/yr to 31 ± 5 mm/yr), and a further decrease at 47.9 Ma (to 17 ± 5 mm/yr) (Fig. 2). In contrast, we do not find a significant change in Pacific-Antarctic spreading direction or rate between ca. 61 and 56 Ma (Fig. 2).

DISCUSSION

Paleocene Farallon Plate Acceleration

We attribute the increase in Pacific-Farallon spreading rates between ca. 58 Ma and ca. 56 Ma to an increase in the absolute speed of Farallon plate motion rather than a change in Pacific plate motion. If a major change in Pacific absolute motion had occurred at this time, we would also expect to see a corresponding significant change in spreading direction or rates for Pacific-Antarctic relative motions; however, no such changes are observed (Fig. 2). The acceleration in Farallon plate motion during this time period roughly marks the end of the Laramide orogeny from ca. 60 Ma (Saleeby, 2003). The Laramide orogeny has been linked with flat-slab subduction (Atwater, 1989; Saleeby, 2003),

[1]GSA Data Repository item 2015156, additional details on our methodology and results, is available online at www.geosociety.org/pubs/ft2015.htm, or on request from editing@geosociety.org or Documents Secretary, GSA, P.O. Box 9140, Boulder, CO 80301, USA.

possibly caused by an increased buoyancy of the oceanic crust due to subduction of oceanic plateaus (i.e., Shatsky and Hess conjugates) on the Farallon plate (Liu et al., 2010). Cessation of Laramide deformation has been linked to rapid steepening of the subducting Farallon slab (Saleeby, 2003) or slab removal (Humphreys et al., 2003). Alternatively, it is proposed that closure of the Mezcalera and Angayucham basins (i.e., by westward movement of North America and west-dipping subduction beneath the arcs) by 55 Ma resulted in terrane accretion (e.g., Siletzia and Metchosin terranes; Sigloch and Mihalynuk, 2013) and development of east-dipping Farallon subduction. In both cases, we expect an increase in Farallon absolute motion, either from steepening of the subducting slab or development of east-dipping subduction.

Farallon Plate Breakup and Vancouver Plate Formation

We suggest that the increase in Farallon absolute plate motion between ca. 58 Ma and ca. 56 Ma would have led to elevated intraplate stress, triggering its breakup and Vancouver plate formation at ca. 52 Ma, given that the Farallon plate already satisfied the main condition for instability of oceanic plates, a plate width larger than the radius of the Earth (Morra et al., 2012). We find a slight decrease from 101 to 93 mm/yr in Pacific-Farallon spreading rates at ca. 52 Ma (Fig. 2), synchronous with the timing of Farallon plate fragmentation. A decrease in Pacific-Farallon spreading rates is an expected consequence of Farallon plate breakup, due to the trench-parallel shortening of the Farallon slab, reducing the slab-pull force. This contrasts with work by Rowan and Rowley (2014), who found an increase in Pacific-Farallon spreading rates at ca. 53 Ma, from 65–97 mm/yr (dependent on spreading asymmetry) to ≥150 mm/yr; however, the difference in their spreading rates is likely a consequence of their ~10-m.y.-long stage intervals, compared to our smaller stages.

Eocene Farallon Plate Acceleration

Pacific-Farallon full spreading rates increased stepwise from ~118 to 180 mm/yr between 49.7 and 40.1 Ma, while Pacific-Antarctic spreading rates decreased slowly and spreading directions rotated counterclockwise by ~22° (Fig. 2), expressed by fracture zone bends (Fig. 1). We suggest that this increase in Pacific-Farallon spreading rates is driven by an eastward acceleration in Farallon absolute plate motion as the Pacific-Farallon ridge approached the trench, since younger oceanic lithosphere may subduct as much as twice as fast as older oceanic lithosphere (Goes et al., 2008). The gradual increase in Pacific-Farallon spreading rates initiating at 49.7 Ma corresponds to the time of inception of the HEB, ca. 50 Ma (O'Connor et al., 2013), and is in contrast with the Barckhausen et al. (2013) suggestion of a singular increase in half-spreading rates from 43 to 89 mm/yr at 47.5 Ma, and the Rowan and Rowley (2014) spreading rate increase at ca. 53 Ma.

The subduction of the Izanagi-Pacific ridge prior to 50 Ma along the western Pacific basin has been associated with initiating a major plate reorganization event in the Pacific basin (Whittaker et al., 2007; Seton et al., 2015). If this were due to a substantial westward acceleration of the Pacific absolute motion due to western Pacific subduction initiation, we would expect a significant acceleration of Pacific-Antarctic spreading rates. We find a decrease in Pacific-Antarctic spreading rates during this time (Fig. 2), suggesting that any change in Pacific absolute motion at this time was relatively minor. Instead, the reorganization may have been driven by the changing plate boundary forces in the western Pacific (from ridge push to slab pull) and the change in mantle flow pattern due to the complete subduction of the Izanagi plate (Seton et al., 2015).

Implications for the Hawaiian-Emperor Bend

The distinct kink in Vancouver-Pacific fracture zones (e.g., Mendocino and Surveyor Fracture Zones) accompanying Farallon plate fragmentation at chron 24 (ca. 52 Ma; Fig. 1B) is related to the reorientation of spreading geometries related to rift propagation (Caress et al., 1988), rather than the HEB and a change in Pacific plate motion. Contemporaneous segments of Pacific-Farallon fracture zones (e.g., Molokai and Clarion Fracture Zones; see Figs. 1C and 1D) preserve linear geometries, suggesting that Pacific-Farallon plate motion is a reliable indicator of steady relative plate motion during this time. Furthermore, a rapid change in Pacific plate motion would also be expressed as a simultaneous change in Pacific-Antarctic motion; however, this is not observed (Fig. 2).

Plate velocity diagrams constructed for the time of formation of the HEB (47.5 Ma) can be used to clarify plate motion changes surrounding this event. We combine our Pacific-Farallon relative motions (in the time scales of Cande and Kent [1995] and Ogg [2012]) with independently derived Pacific absolute motion models: (1) a geodynamic forward-based model (Butterworth et al., 2014) (Fig. 3A), (2) a Pacific hotspot model corrected for the southward motion of the Hawaiian hotspot (WK08-D; Chandler et al., 2012) (Fig. 3B), and (3) a smoothed Pacific absolute plate motion model uncorrected for Hawaiian hotspot drift (WK08-A; Wessel and Kroenke, 2008) (Fig. 3C). Regardless of the time scale used, all models suggest an acceleration in Farallon plate absolute motion (Fig. 3), which includes a minor clockwise change. This may be attributed to the detachment of the Vancouver plate at ca. 52 Ma, causing slab pull forces associated with the South American trench to become more dominant. Both Chandler et al. (2012; WK08-D; Fig. 3B) and Butterworth et al. (2014) (Fig. 3A) suggested a slight deceleration in Pacific absolute motion around the formation time of the HEB, with little accompanying change in direction (4° clockwise and 5° counterclockwise, respectively). Wessel and Kroenke (2008; WK08-A; Fig. 3C) implied a 31° counterclockwise change and acceleration in Pacific plate absolute motion, in order to reproduce the HEB without attempting to separate absolute plate motion change from plume motion. This suggests that the HEB is largely due to the cessation of the rapid southward motion of the Hawaiian hotspot around the formation time of the HEB (Tarduno et al., 2003), rather than a large change in Pacific absolute motion or a basin-wide plate reorganization event.

The lack of statistically significant change in Pacific-Farallon spreading directions, combined with a significant increase in Pacific-Farallon

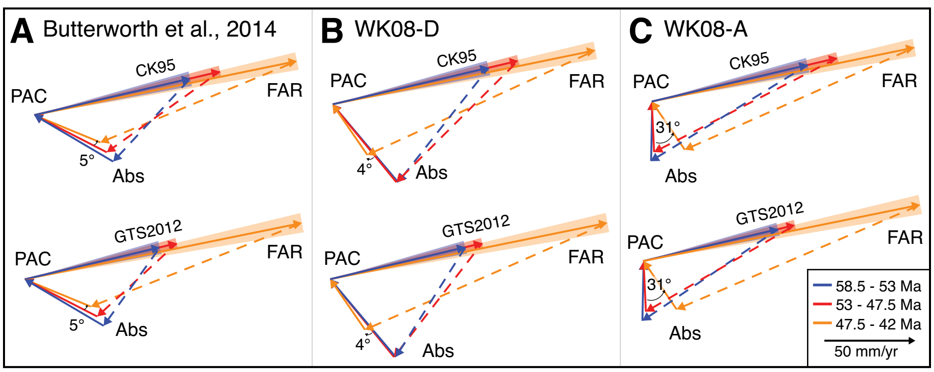

Figure 3. Plate velocity diagrams surrounding the formation of the Hawaiian-Emperor bend (HEB) (47.5 Ma) based on relative Pacific (PAC)-Farallon (FAR) motion (solid line, with uncertainty shaded) in the time scales of Cande and Kent (1995; CK95) and Ogg (2012; GTS2012), Pacific absolute (abs) motion (solid line), and Farallon absolute motion (dashed line). A: Pacific absolute motion from Butterworth et al. (2014). B: Pacific absolute motion from model WK08-D (Chandler et al., 2012). C: Pacific absolute motion from model WK08-A (Wessel and Kroenke, 2008). Uncertainties in all parts are derived from a similar time period in this study. All velocities were calculated at the paleo-ridge along the Murray Fracture Zone.

spreading rates and a gradual deceleration of Pacific-Antarctic spreading rates, suggests that there was no major change in Pacific plate absolute motion around the formation time of the HEB (47.5 Ma). The increase in Pacific-Farallon spreading rates can be attributed to changes in Farallon plate absolute motion. Our analysis supports the scenario that the rapid southward motion of the Hawaiian hotspot until ca. 47 Ma is responsible for the HEB, rather than a change in Pacific absolute motion.

ACKNOWLEDGMENTS

We thank M. Croon, S. Cande, and J. Stock for making their Hellinger plate reconstruction input files available to us. We also thank Charles DeMets and four anonymous reviewers for comments that significantly improved this manuscript. This research was funded by Australian Research Council grants FL0992245 and DP0987713.

REFERENCES CITED

Atwater, T., 1989, Plate tectonic history of the northeast Pacific and western North America, *in* Winterer, E.L., et al., eds., The eastern Pacific Ocean and Hawaii: Boulder, Colorado, Geological Society of America, Geology of North America, v. N, p. 21–72.

Barckhausen, U., Bagge, M., and Wilson, D.S., 2013, Seafloor spreading anomalies and crustal ages of the Clarion-Clipperton Zone: Marine Geophysical Researches, v. 34, p. 79–88, doi:10.1007/s11001-013-9184-6.

Butterworth, N.P., Müller, R.D., Quevedo, L., O'Connor, J.M., Hoernle, K., and Morra, G., 2014, Pacific plate slab pull and intraplate deformation in the early Cenozoic: Solid Earth, v. 5, p. 757–777, doi:10.5194/se-5-757-2014.

Cande, S.C., and Haxby, W.F., 1991, Eocene propagating rifts in the southwest Pacific and their conjugate features on the Nazca plate: Journal of Geophysical Research, v. 96, p. 19,609–19,622, doi:10.1029/91JB01991.

Cande, S.C., and Kent, D.V., 1995, Revised calibration of the geomagnetic polarity time scale for the Late Cretaceous and Cenozoic: Journal of Geophysical Research, v. 100, p. 6093–6095, doi:10.1029/94JB03098.

Cande, S.C., Raymond, C.A., Stock, J., and Haxby, W.F., 1995, Geophysics of the Pitman Fracture Zone and Pacific-Antarctic plate motions during the Cenozoic: Science, v. 270, p. 947–953, doi:10.1126/science.270.5238.947.

Caress, D.W., Menard, H., and Hey, R., 1988, Eocene reorganization of the Pacific-Farallon spreading center north of the Mendocino Fracture Zone: Journal of Geophysical Research, v. 93, p. 2813–2838, doi:10.1029/JB093iB04p02813.

Chandler, M.T., Wessel, P., Taylor, B., Seton, M., Kim, S.S., and Hyeong, K., 2012, Reconstructing Ontong Java Nui: Implications for Pacific absolute plate motion, hotspot drift and true polar wander: Earth and Planetary Science Letters, v. 331, p. 140–151, doi:10.1016/j.epsl.2012.03.017.

Croon, M.B., Cande, S.C., and Stock, J.M., 2008, Revised Pacific-Antarctic plate motions and geophysics of the Menard Fracture Zone: Geochemistry, Geophysics, Geosystems, v. 9, Q07001, doi:10.1029/2008GC002019.

Doubrovine, P.V., and Tarduno, J.A., 2008. A revised kinematic model for the relative motion between Pacific oceanic plates and North America since the Late Cretaceous: Journal of Geophysical Research, v .113, B12101, doi:10.1029/2008JB005585.

Goes, S., Capitanio, F.A., and Morra, G., 2008, Evidence of lower-mantle slab penetration phases in plate motions: Nature, v. 451, p. 981–984, doi:10.1038/nature06691.

Humphreys, E., Hessler, E., Dueker, K., Farmer, G.L., Erslev, E., and Atwater, T., 2003, How Laramide-age hydration of North American lithosphere by the Farallon slab controlled subsequent activity in the western United States: International Geology Review, v. 45, p. 575–595, doi:10.2747/0020-6814.45.7.575.

Koivisto, E.A., Andrews, D.L., and Gordon, R.G., 2014, Tests of fixity of the Indo-Atlantic hot spots relative to Pacific hot spots: Journal of Geophysical Research, v. 119, p. 661–675, doi:10.1002/2013JB010413.

Liu, L., Gurnis, M., Seton, M., Saleeby, J., Müller, R.D., and Jackson, J.M., 2010, The role of oceanic plateau subduction in the Laramide orogeny: Nature Geoscience, v. 3, p. 353–357, doi:10.1038/ngeo829.

Matthews, K.J., Müller, R.D., Wessel, P., and Whittaker, J.M., 2011, The tectonic fabric of the ocean basins: Journal of Geophysical Research, v. 116, B12109, doi:10.1029/2011JB008413.

Morra, G., Quevedo, L., and Müller, R., 2012, Spherical dynamic models of top-down tectonics: Geochemistry, Geophysics, Geosystems, v. 13, Q03005, doi:10.1029/2011GC003843.

Müller, R.D., Sandwell, D.T., Tucholke, B.E., Sclater, J.G., and Shaw, P.R., 1991, Depth to basement and geoid expression of the Kane Fracture Zone: A comparison: Marine Geophysical Researches, v. 13, p. 105–129, doi:10.1007/BF00286284.

Norton, I.O., 1995, Plate motions in the North Pacific: The 43 Ma nonevent: Tectonics, v. 14, p. 1080–1094, doi:10.1029/95TC01256.

O'Connor, J.M., Steinberger, B., Regelous, M., Koppers, A.A., Wijbrans, J.R., Haase, K.M., Stoffers, P., Jokat, W., and Garbe-Schönberg, D., 2013, Constraints on past plate and mantle motion from new ages for the Hawaiian-Emperor Seamount Chain: Geochemistry, Geophysics, Geosystems, v. 14, p. 4564–4584, doi:10.1002/ggge.20267.

Ogg, J.G., 2012, Geomagnetic polarity time scale, *in* Gradstein, F.M., et al., eds., The geologic time scale 2012: Boston, USA, Elsevier, p. 85–114, doi:10.1016/B978-0-444-59425-9.00005-6.

Rowan, C.J., and Rowley, D.B., 2014, Spreading behaviour of the Pacific-Farallon ridge system since 83 Ma: Geophysical Journal International, v. 197, p. 1273–1283, doi:10.1093/gji/ggu056.

Royer, J.Y., and Chang, T., 1991, Evidence for relative motions between the Indian and Australian plates during the last 20 my from plate tectonic reconstructions: Implications for the deformation of the Indo-Australian plate: Journal of Geophysical Research, v. 96, p. 11,779–11,802, doi:10.1029/91JB00897.

Saleeby, J., 2003, Segmentation of the Laramide slab—Evidence from the southern Sierra Nevada region: Geological Society of America Bulletin, v. 115, p. 655–668, doi:10.1130/0016-7606(2003)115<0655:SOTLSF>2.0.CO;2.

Seton, M., et al., 2014, Community infrastructure and repository for marine magnetic identifications: Geochemistry, Geophysics, Geosystems, v. 15, p. 1629–1641, doi:10.1002/2013GC005176.

Seton, M., Flament, N., Whittaker, J., Müller, R.D., Gurnis, M., and Bower, D.J., 2015, Ridge subduction sparked reorganisation of the Pacific plate-mantle system 60–50 million years ago: Geophysical Research Letters, doi:10.1002/2015GL063057 (in press).

Sharp, W.D., and Clague, D.A., 2006, 50-Ma initiation of Hawaiian-Emperor bend records major change in Pacific plate motion: Science, v. 313, p. 1281–1284, doi:10.1126/science.1128489.

Sigloch, K., and Mihalynuk, M.G., 2013, Intra-oceanic subduction shaped the assembly of Cordilleran North America: Nature, v. 496, p. 50–56, doi:10.1038/nature12019.

Steinberger, B., Sutherland, R., and O'Connell, R.J., 2004, Prediction of Emperor-Hawaii seamount locations from a revised model of global plate motion and mantle flow: Nature, v. 430, p. 167–173, doi:10.1038/nature02660.

Tarduno, J.A., 2007, On the motion of Hawaii and other mantle plumes: Chemical Geology, v. 241, p. 234–247, doi:10.1016/j.chemgeo.2007.01.021.

Tarduno, J.A., et al., 2003, The Emperor Seamounts: Southward motion of the Hawaiian hotspot plume in Earth's mantle: Science, v. 301, p. 1064–1069, doi:10.1126/science.1086442.

Tarduno, J.A., Bunge, H.P., Sleep, N., and Hansen, U., 2009, The bent Hawaiian-Emperor hotspot track: Inheriting the mantle wind: Science, v. 324, p. 50–53, doi:10.1126/science.1161256.

Wessel, P., and Kroenke, L.W., 2008, Pacific absolute plate motion since 145 Ma: An assessment of the fixed hot spot hypothesis: Journal of Geophysical Research, v. 113, B06101, doi:10.1029/2007JB005499

Whittaker, J.M., Müller, R.D., Leitchenkov, G., Stagg, H., Sdrolias, M., Gaina, C., and Goncharov, A., 2007, Major Australian-Antarctic plate reorganization at Hawaiian-Emperor bend time: Science, v. 318, p. 83–86, doi:10.1126/science.1143769.

Manuscript received 23 September 2014
Revised manuscript received 25 February 2015
Manuscript accepted 3 March 2015

Printed in USA

GSA DATA REPOSITORY

Revision of Paleogene plate motions in the Pacific and implications for the Hawaiian-Emperor bend

N. M. Wright, R. D. Müller, M. Seton, S. E. Williams

Methodology

Data compilation

We rely on magnetic identifications compiled by Seton et al. (2014) and fracture zone crossings determined by Matthews et al. (2011). Specifically, for our Pacific-Farallon reconstructions we rely on magnetic identifications from Atwater and Severinghaus (1989), Barckhausen et al. (2013), Cande and Haxby (1991), Cande et al. (1995), Caress et al. (1988), Elvers et al. (1967), Munschy et al. (1996), and Vacquier et al. (1961). For our Pacific-Antarctic reconstruction, we rely on Cande et al. (1995) and Wobbe et al. (2012).

All magnetic identifications compiled by Seton et al. (2014) are standardized to the Gee and Kent (2007) timescale. We cite such ages as Cande and Kent (1995), from which the Cenozoic portion of the Gee and Kent (2007) magnetic timescale is based. We identify chrons based on their young (y), old (o), and middle (m) ends.

Reconstruction method

Uncertainty analysis

We assign a 5 km uncertainty to fracture zone identifications (Müller et al., 1991). Since our magnetic identifcation compilation is based on different navigation methods, including celestial navigation (i.e. for pre-1970 data), we rely on the dispersion of magnetic identifications in assigning their uncertainty value (Gaina et al., 1998). This uncertainty value is found by (1) initially finding the best fitting rotations for all data (magnetic and fracture zone crossings); (2) applying these rotations only to magnetic crossings with an assigned initial uncertainty (10 km); (3) calculating the harmonic mean of the quality factor $\hat{\kappa}$ (i.e. $\hat{\kappa}_{\text{avg}}$), based the $\hat{\kappa}$ values of each magnetic anomaly set; and (4) determining the 1-sigma standard error (σ) of the magnetic data, based on $\sigma = \hat{\sigma} \, / \, \sqrt{\hat{\kappa}}_{\text{avg}}$, which we assign as our magnetic uncertianty. For Pacific-Farallon/Vancouver rotations, we find $\hat{\kappa}_{\text{avg}}$ of 1.6 and σ of 7.8 km. For Pacific-Antarctic rotations, we find we find $\hat{\kappa}_{\text{avg}}$ of 2.1 and σ of 6.9 km.

'Half'-stage rotations

Half-stage rotation poles and uncertainties were obtained based on preserved magnetic lineations on the Pacific plate and Hellinger's (1981) best-fitting method, implemented by Chang (1987, 1988) and Royer and Chang (1991). We derived Pacific-Farallon half-stage rotation poles and 95% uncertainties (Fig. DR1A) between chron 13y (33.058 Ma) and chron 24n.1y (52.364 Ma) (Table DR1, Table DR2), based on magnetic identifications south of the Murray Fracture Zone. We derive Vancouver-Pacific rotations and 95% uncertainties (Fig. DR1B) between chron 13y (33.058 Ma) and chron 24n.1y (52.364 Ma) (Table DR1, Table DR2) based on magnetic identifications north of the Mendocino Fracture Zone. We derive Pacific-Farallon/Vancouver rotations (i.e. pre-Vancouver plate formation) and 95% uncertainties (Fig. DR1) between chron 24n.1y (52.364 Ma) and chron

31y (67.735 Ma) (Table DR1, Table DR2). Our obtained half-stage rotations are independent of Nazca plate formation (e.g. at ~23 Ma; Barckhausen et al., 2008), as this spreading occurred prior to Farallon plate breakup and we derive half-stage rotations only.

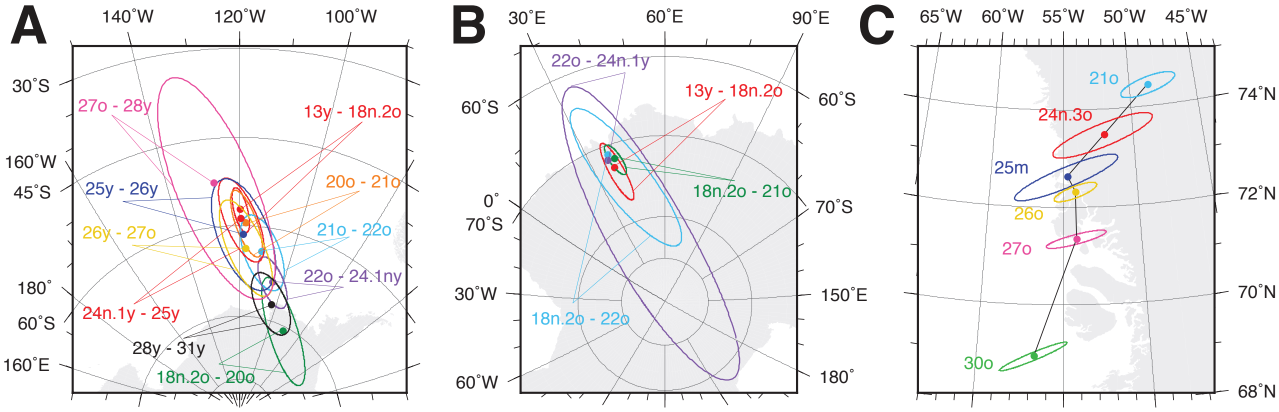

Figure DR1: Rotation poles and their corresponding 95% uncertainty regions, for A. Farallon-Pacific spreading (half-stage poles); B. Vancouver-Pacific spreading (half-stage poles). C. Pacific-Antarctic (finite poles). Labels denote chrons used for computation.

Table DR1: Chron and ages of half-stage rotations for Farallon-Pacific, Vancouver-Pacific, and Farallon/Vancouver-Pacific spreading. Ages are from Cande and Kent (1995)

Plates	Chron	Age (Ma)
Farallon - Pacific	13y - 18n.2o	33.058 - 40.130
	18n.2o - 20o	40.130 - 43.789
	20o - 21o	43.789 - 47.906
	21o - 22o	47.906 - 49.714
	22o - 24n.1y	49.714 - 52.364
Vancouver - Pacific	13y - 18n.2o	33.058 - 40.130
	18n.2o - 21o	40.130 - 47.906
	21o - 22o	47.906 - 49.714
	21o - 24n.1y	49.714 - 52.364
Farallon/Vancouver - Pacific	24n.1y - 25y	52.364 - 55.904
	25y - 26y	55.904 - 57.554
	26y - 27o	57.554 - 61.276
	27o - 28y	61.276 - 62.499
	28y - 31y	62.499 - 67.735

Table DR2: Farallon-Pacific (FAR-PAC), Vancouver-Pacific (VAN-PAC), and Farallon/Vancouver-Pacific (FAR/VAN-PAC) half-stage rotation and covariance matrices

Plates	Chron	Lat (+ °N)	Long (+ °E)	Angle (deg)	$\hat{\kappa}$	*dF*	*N*	*s*	*r*	*a*	*b*	*c*	*d*	*e*	*f*	*g*
FAR-PAC	13y - 18n.2o	-57.206	-119.683	5.796	0.24	51	76	11	208.82	8.49	8.83	0.24	11.90	0.27	1.90	10^{-7}
	18n.2o - 20o	-75.751	-90.302	2.765	0.30	51	74	10	172.34	10.45	9.08	-3.62	10.32	-3.58	2.94	10^{-7}
	20o - 21o	-59.482	-117.813	2.653	0.35	76	107	14	215.39	6.08	4.57	-1.72	4.95	-1.51	1.52	10^{-7}
	21o - 22o	-64.069	-111.485	0.954	0.99	105	138	15	105.87	3.20	2.11	-0.15	2.81	-0.24	0.68	10^{-7}
	22o - 24n.1y	-68.840	-104.776	1.147	3.19	57	80	10	17.86	6.18	3.79	-1.45	4.61	-1.30	1.61	10^{-7}
VAN-PAC	13y - 18n.2o	-72.935	38.385	7.125	0.44	66	85	8	149.22	1.50	62.31	-80.15	30.99	-55.53	106.40	10^{-7}
	18n.2o – 21o	-71.865	39.600	6.217	1.41	49	66	7	34.78	0.84	50.59	-59.96	21.29	-37.24	74.96	10^{-7}
	21o – 22o	-71.145	37.555	1.319	2.32	35	52	7	15.06	0.66	78.03	-89.57	23.54	-47.23	107.24	10^{-7}
	21o - 24n.1y	-71.810	36.938	1.454	0.91	25	40	6	27.34	1.05	82.19	-93.96	36.53	-62.02	114.18	10^{-7}
FAR/VAN-PAC	24n.1y - 25y	-58.818	-119.609	1.591	0.60	71	96	11	118.99	6.58	4.17	-1.88	4.50	-1.51	1.65	10^{-7}
	25y – 26y	-61.494	-118.605	0.571	1.49	118	151	15	79.16	3.32	1.62	-1.70	2.15	-1.30	1.74	10^{-7}
	26y - 27o	-63.787	-117.523	1.177	0.87	87	114	12	99.97	6.28	3.34	-3.36	3.46	-2.31	2.87	10^{-7}
	27o - 28y	-52.581	-127.173	0.374	1.51	89	118	13	58.90	6.26	3.48	-3.34	3.36	-2.26	2.81	10^{-7}
	28y – 31y	-72.402	-102.630	1.881	0.61	122	145	10	198.70	4.84	2.05	-2.95	2.81	-2.01	2.82	10^{-7}

Variables $\hat{\kappa}, a, b, c, d, e$ and f are in radians. $\hat{\kappa}$ is the estimated quality factor, *dF* is number of degrees of freedom, *N* is the number of datapoints, *s* is the number of great circle segments, *r* is the total misfit

The covariance matrix is defined as: $Cov(u) = \frac{g}{\hat{\kappa}} \begin{pmatrix} a & b & c \\ b & d & e \\ c & e & f \end{pmatrix}$

The quality factor $\hat{\kappa}$ value indicates whether our assigned uncertainties are relatively correct ($\hat{\kappa}$ = 1), overestimated ($\hat{\kappa}$ >> 1) or underestimated ($\hat{\kappa}$ << 1). Our $\hat{\kappa}$ values varied between 0.24 and 3.19 for our derivations (Table DR2). We chose to retain our assigned uncertainties. We transformed these 'half'-stage rotation poles into stage poles (assuming symmetrical spreading) and derived finite rotation poles using ADDPLUS (Kirkwood et al., 1999). To assess our rotations, we visualised our finite rotations as flowlines using *GPlates* (Boyden et al., 2011).

We present our Farallon-Pacific spreading velocities in Cande and Kent (1995) (Fig. DR2A, B) and Ogg (2012) (Fig DR2C, D). We find a well-constrained increase in spreading rate at ca. 57 - 56 Ma in both timescales. To account for the long term spreading asymmetry of the East-Pacific rise (EPR) and its ancestor, Pacific-Farallon ridge (Rowan and Rowley, 2014), we additionally calculate full stage rotations based on two spreading asymmetry cases: 1) 'best-fitting' asymmetry, with a Pacific:Farallon spreading asymmetry of 44:56 for all stages (Rowan and Rowley, 2014), and 2) maximum likely asymmetry, with a Pacific:Farallon spreading asymmetry of 36:64 for stages before chron 24, and 44:56 for stages since chron 24 (Rowan and Rowley, 2014) (Fig DR2). A comparison with the 'best-fit' rotation poles from Rowan and Rowley (2014) demonstrates a similar overall trend, although we find an earlier increase in Pacific-Farallon spreading rates due to our smaller stage rotations.

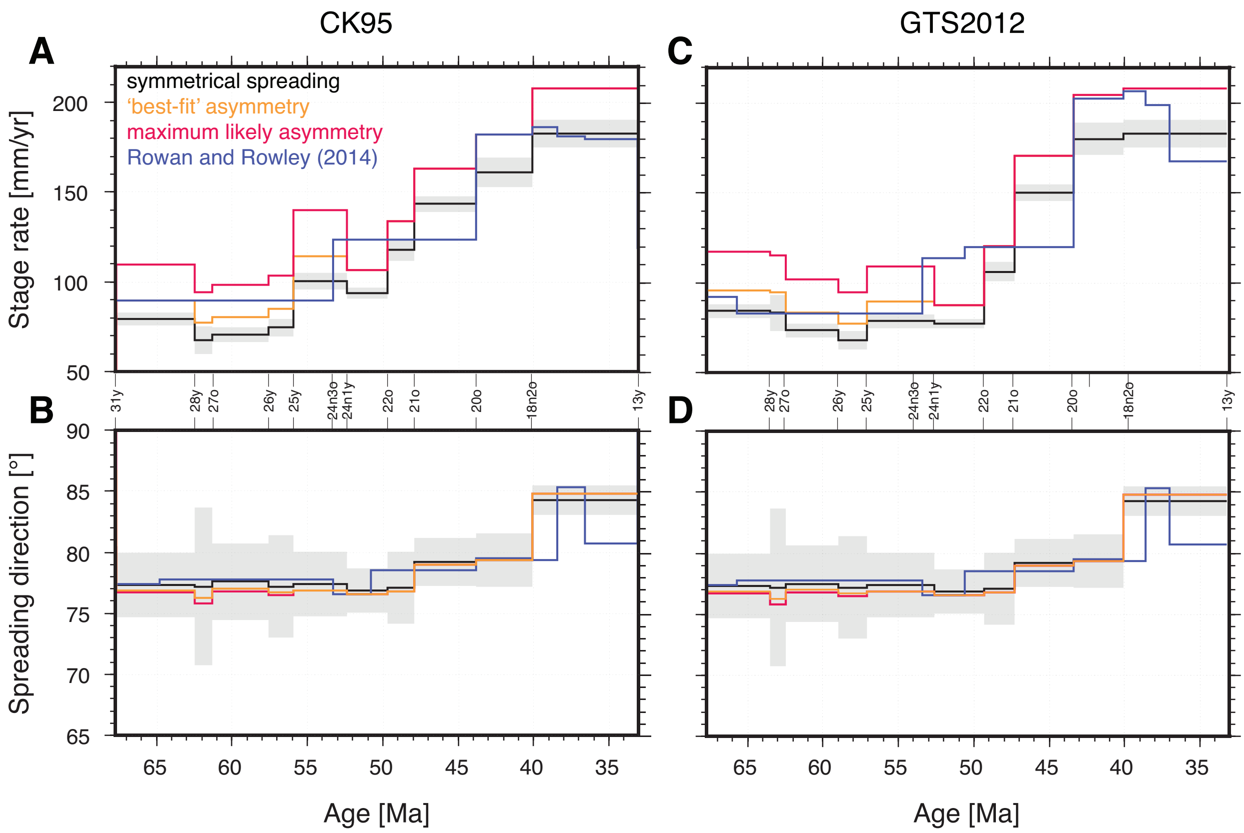

Figure DR2: Comparison of Pacific-Farallon spreading velocities in A and B: Cande and Kent (1995) ('CK95') and C and D: Ogg (2012) ('GTS2012'). Stage rates have been calculated based on symmetrical spreading (black), 'best-fit' asymmetry (yellow), and maximum likely asymmetry (red). A comparison is provided based on Rowan and Rowley's (2014) preferred rotations poles.

Due to the sensitivity of the use of Hellinger's (1981) method in half-stage cases, significant differences in boundary segment trends (e.g. due to propagating ridges and transform faults) will result in a non-Gaussian distribution. We verify the distribution by plotting both histograms of the residual distribution (by stage) and normal quantile plots (qq plot; for combined dataset from all stages). If the data residuals are normally distributed, all points on a qq plot should lie on a straight line. We find a Gaussian distribution of our residuals for all half-stage rotations (Fig. DR3), and an approximately linear distribution in qq plots (Fig. DR4).

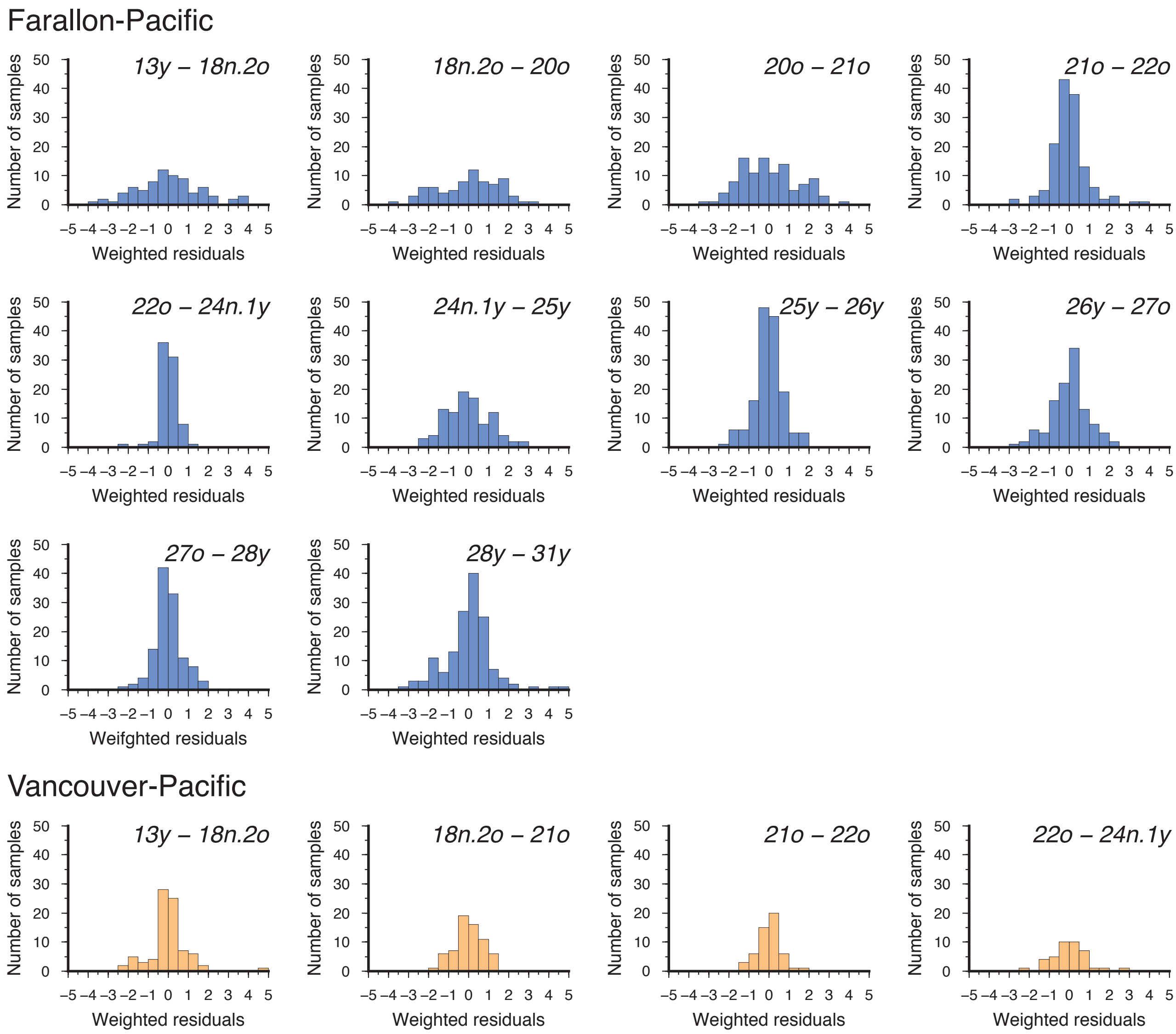

Figure DR3: Histograms of weighted residual distributions from Farallon-Pacific and Farallon/Vancouver-Pacific half-stage rotations (blue) and Vancouver-Pacific half-stage rotations (orange).

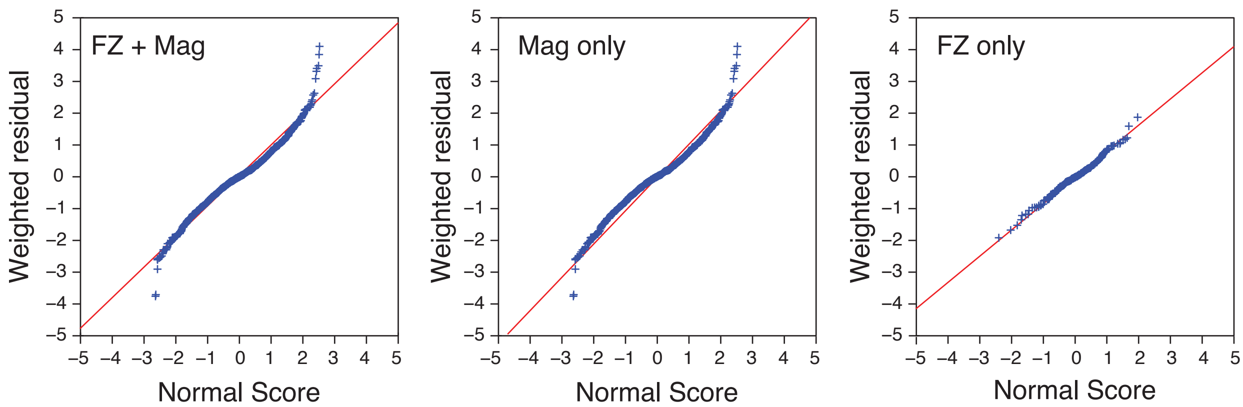

Figure DR4: qq-plots based on combined Farallon-Pacific, Vancouver-Pacific and Farallon/Vancouver-Pacific half-stage poles, based on the full dataset, magnetic anomaly data only, and fracture zone data only.

Finite rotations

Finite rotation poles were obtained based on preserved magnetic lineations on the Antarctic and Pacific plates. We derive Pacific-Antarctic finite rotations and 95% uncertainties (Fig. DR1C) between chron 21o (47.906 Ma) and chron 30o (67.610 Ma) (Table DR3, Table DR4). We rely on Croon et al. (2008) for spreading rates and uncertainties for times since chron 20o (43.789 Ma).

Table DR3: Chron and ages of finite rotations for Pacific-Antarctic spreading. Ages are from Cande and Kent (1995)

Chron	Age (Ma)
21o	47.906
24n.3o	53.347
25m	56.1475
26o	57.911
27o	61.276
30o	67.610

Table DR4: Finite rotations and covariance matrix for Pacific-Antarctic spreading

Chron	Lat (+ °N)	Long (+ °E)	Angle (deg)	$\hat{\kappa}$	*df*	*N*	*s*	*r*	*a*	*b*	*c*	*d*	*e*	*f*	*g*
21o	74.431	-48.544	38.176	0.37	37	56	8	100.11	0.24	0.05	0.37	0.02	0.08	0.62	10^{-5}
24n.3o	73.474	-52.081	40.105	0.21	19	38	8	92.60	0.49	0.06	0.79	0.03	0.09	1.34	10^{-5}
25m	72.627	-54.727	41.142	0.36	18	35	7	49.40	0.87	0.16	1.21	0.06	0.22	1.76	10^{-5}
26o	72.317	-54.189	42.531	0.67	23	48	11	34.20	0.35	0.02	0.55	0.02	0.02	0.93	10^{-5}
27o	71.348	-54.157	45.498	1.25	31	44	5	24.78	1.84	-0.21	3.00	0.04	-0.33	5.00	10^{-5}
30o	68.941	-56.694	49.007	2.76	16	31	6	5.79	4.95	-0.26	7.47	0.06	-0.40	11.39	10^{-5}

Variables $\hat{\kappa}, a, b, c, d, e$ and f are in radians. $\hat{\kappa}$ is the estimated quality factor, *dF* is number of degrees of freedom, *N* is the number of datapoints, *s* is the number of great circle segments, *r* is the total misfit

The covariance matrix is defined as: $Cov(u) = \frac{g}{\hat{\kappa}} \begin{pmatrix} a & b & c \\ b & d & e \\ c & e & f \end{pmatrix}$

Our final $\hat{\boldsymbol{\kappa}}$ values range from 0.21 to 2.76 (Table DR4), indicating we have overestimated uncertainties (e.g. chron 30o) and underestimated uncertainties (e.g. chron 21o). We find a Gaussian distribution of our residuals (Figure DR5), and a linear distribution in our qq-plots (Figure DR6).

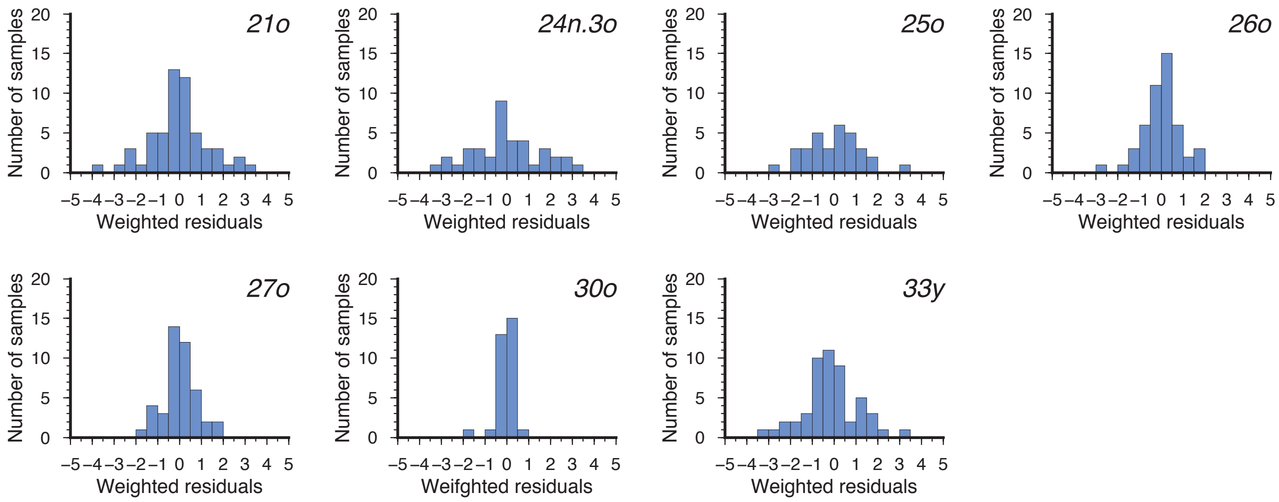

Figure DR5: Histograms of weighted residual distribution from Pacific-Antarctic rotations

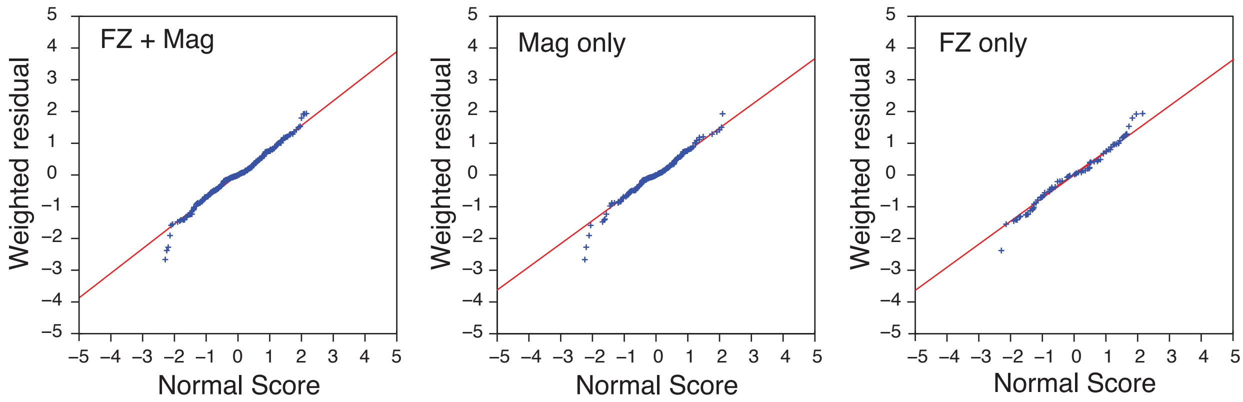

Figure DR6: qq-plots based for Pacific-Antarctic rotations, based on the full dataset, magnetic anomaly data only, and fracture zone data only.

95% uncertainty ellipses

Figure DR7 displays the velocity arrows and uncertainty ellipses for each Farallon/Vancouver-Pacific half-stage described in the text. Gravity is from Sandwell and Smith (2009), plate boundaries are from Bird (2003), and magnetic identifications are from Matthews et al. (2011). Chrons include: 13y (33.058 Ma; peach), 18n.2o (40.103 Ma; green), 20o (43.789 Ma; orange), 21o (47.906 Ma; light blue), 22o (49.714 Ma; purple), 24n.1y (52.364 Ma; dark red), 25y (55.904 Ma; dark blue), 26y (57.554 Ma; gold), 27o (61.276 Ma; pink), 28y (62.499 Ma; black) and 31y (67.735 Ma; pale yellow).

Figure DR8 displays the velocity arrows and uncertainty ellipses for Pacific-Antarctic spreading, based on full stages. Accordingly, the velocity arrows will be twice as long as the half-stage arrows, and will not align with the equivalent chron associated with each stage rotation. Chrons include: 21o (47.906 Ma; light blue), 24n.3o (53.347 Ma; dark red), 25m (56.1475 Ma; off-white), 26o (57.911 Ma; gold), 27o (61.276 Ma; pink), and 30o (67.610 Ma; yellow).

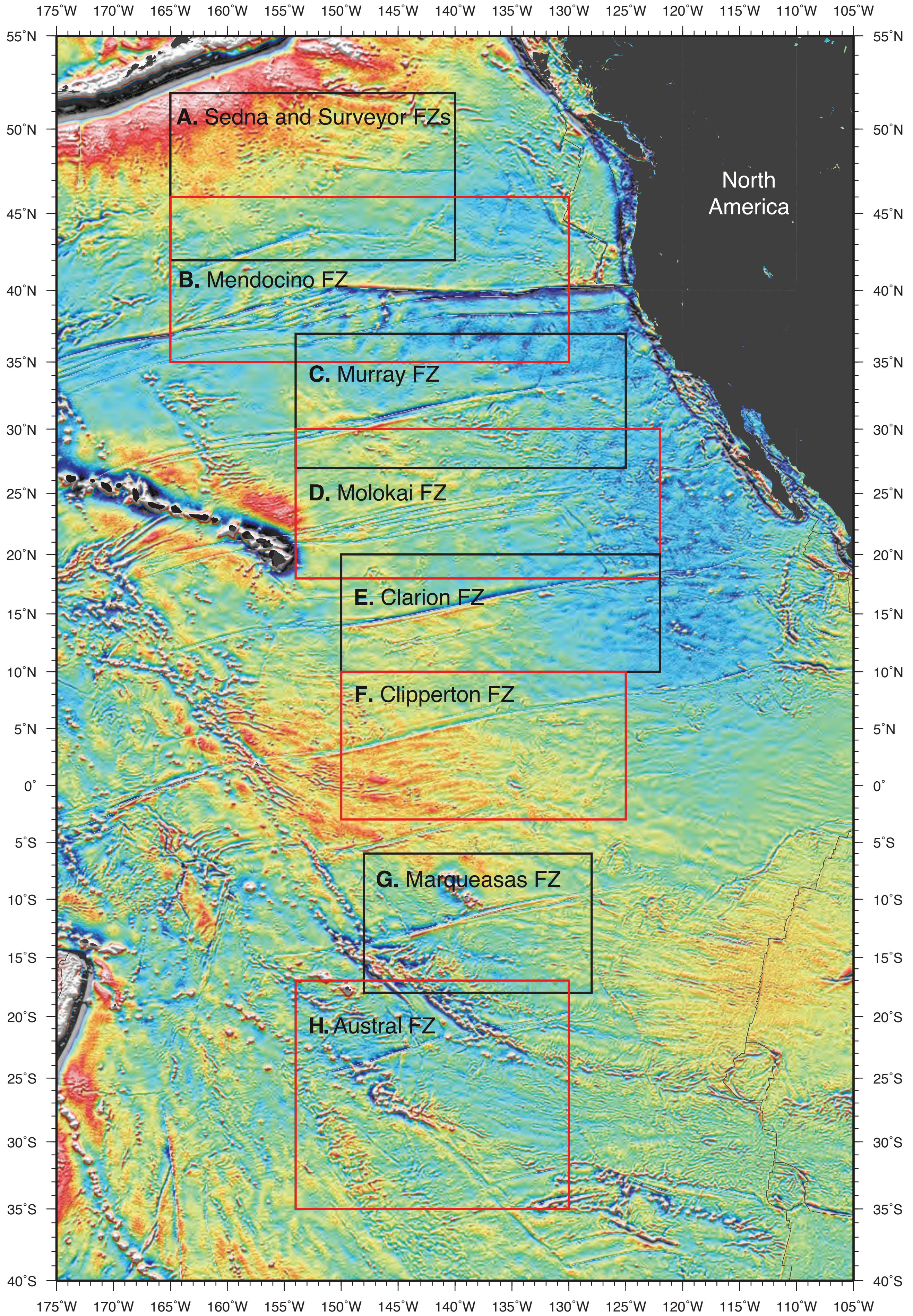

Figure DR7: Overview of regions in sections A - H

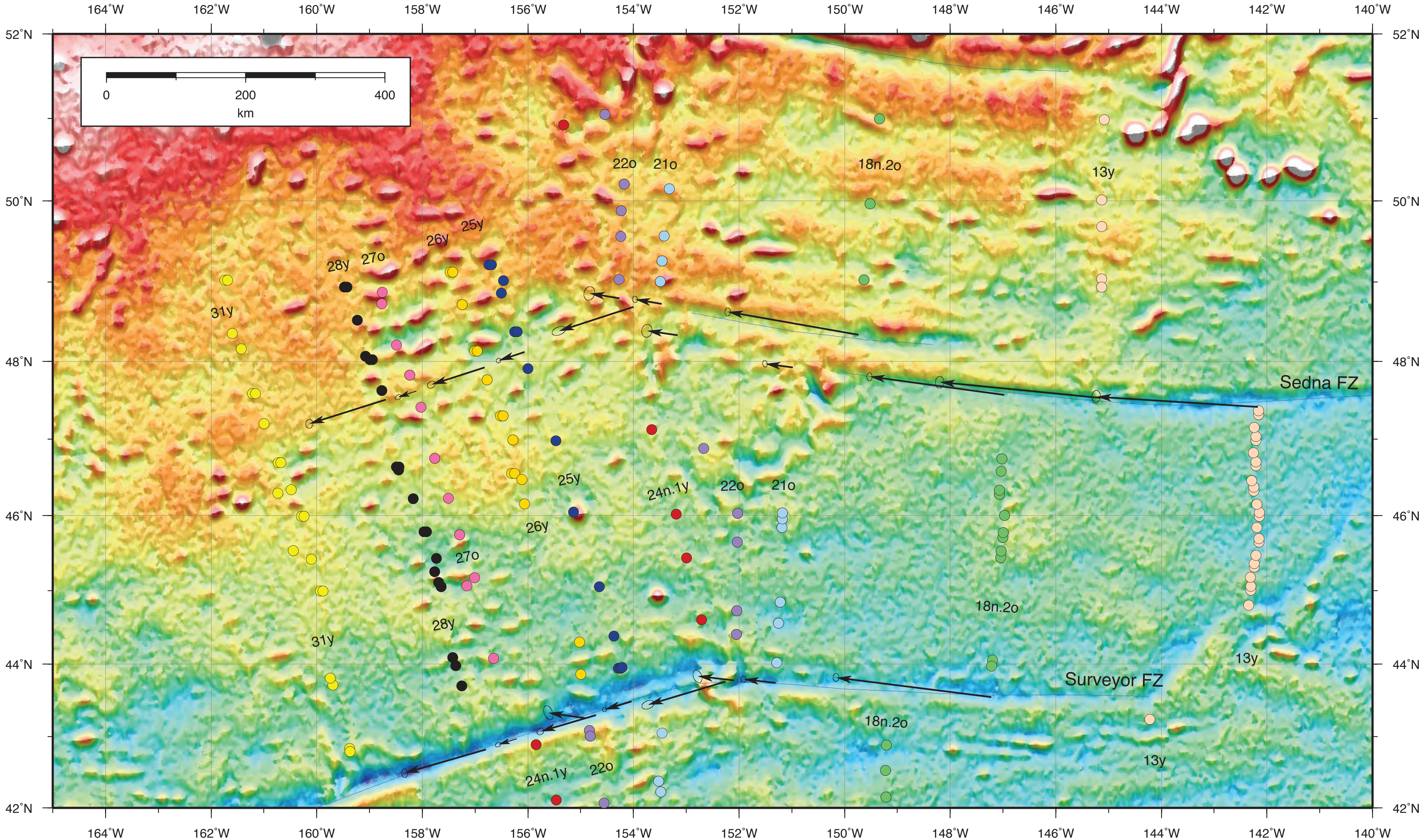

Figure DR7A: Sedna and Surveyor Fracture Zones

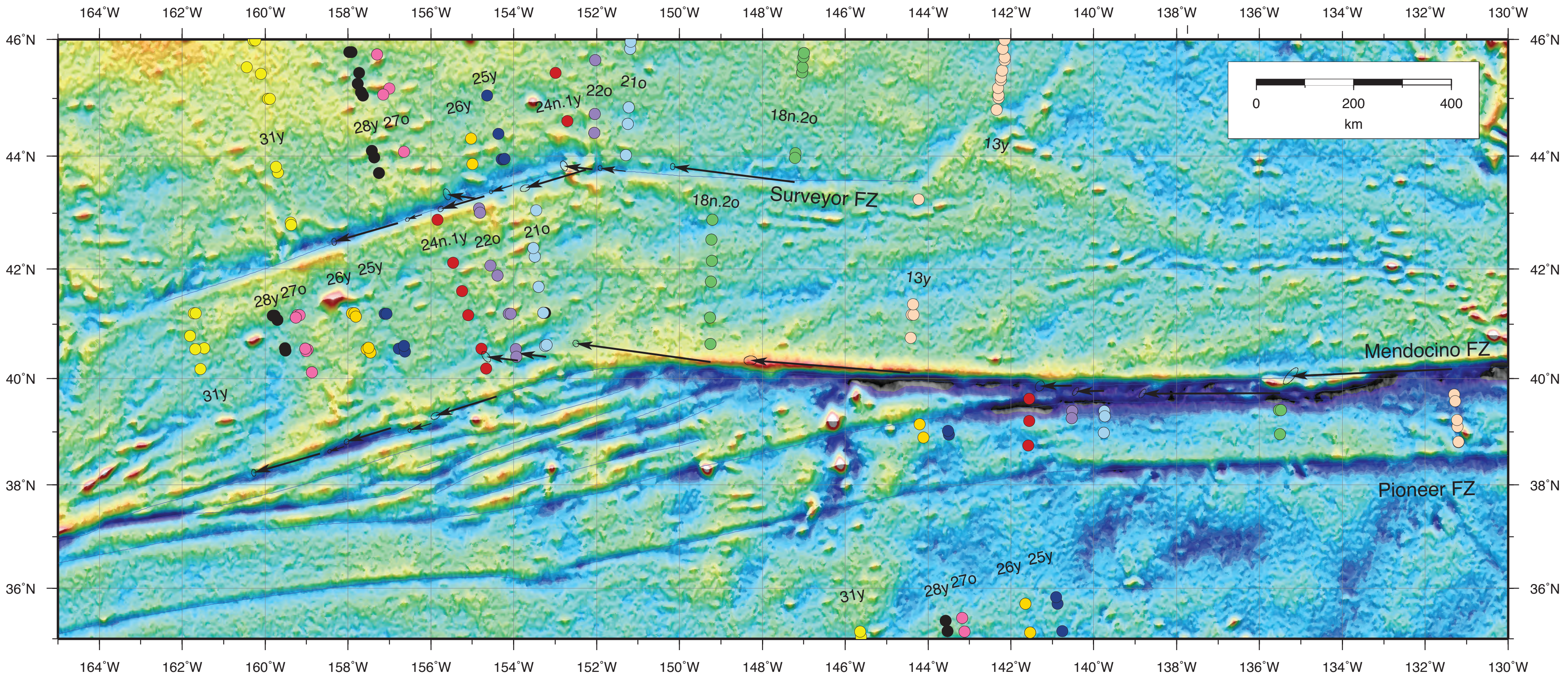

Figure DR7B: Mendocino Fracture Zone

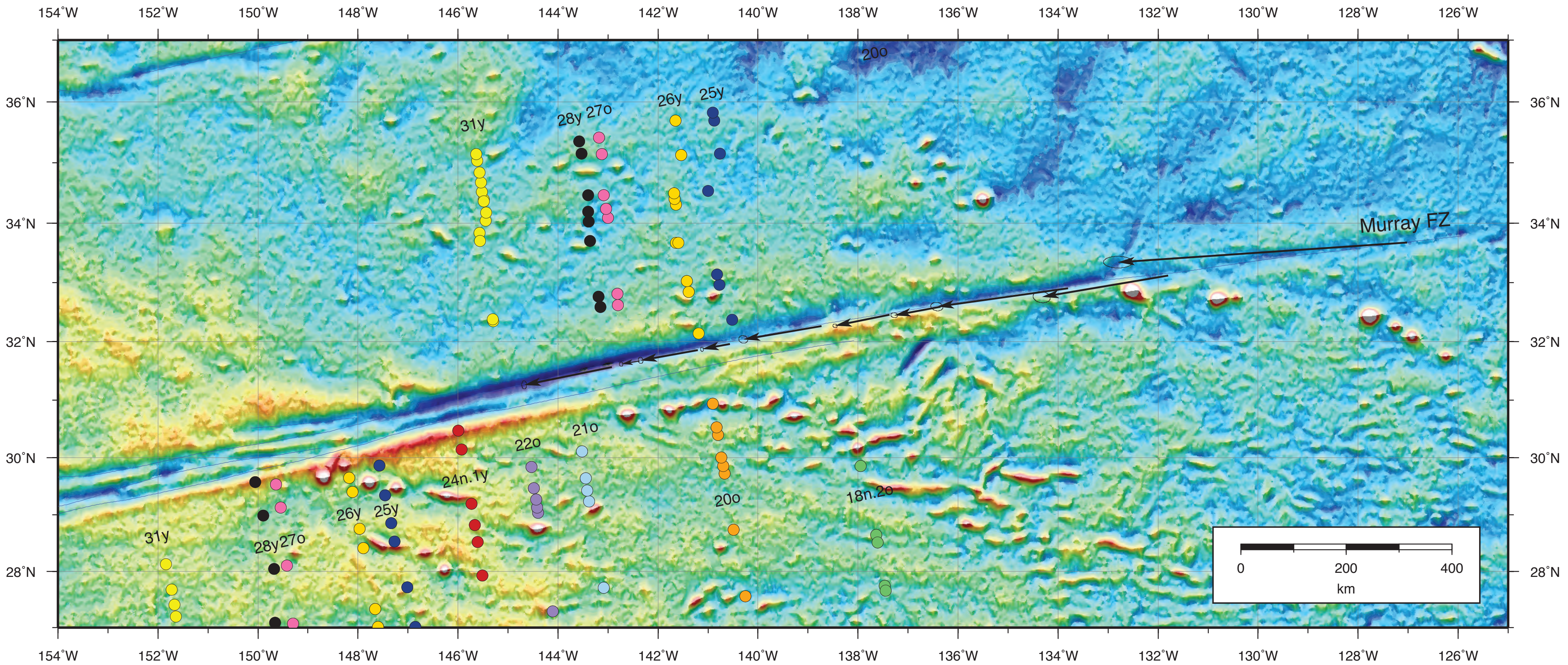

Figure DR7C: Murray Fracture Zone

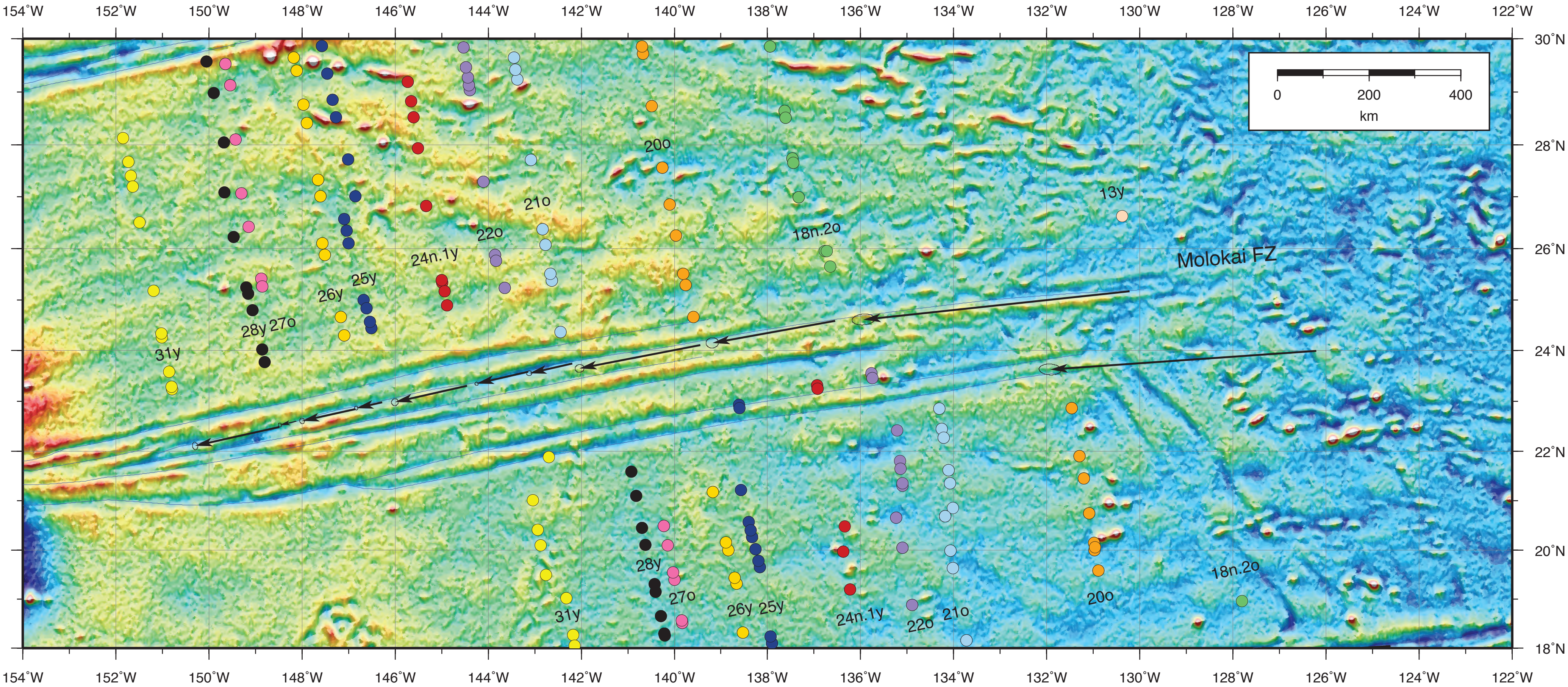

Figure DR7D: Molokai Fracture Zone

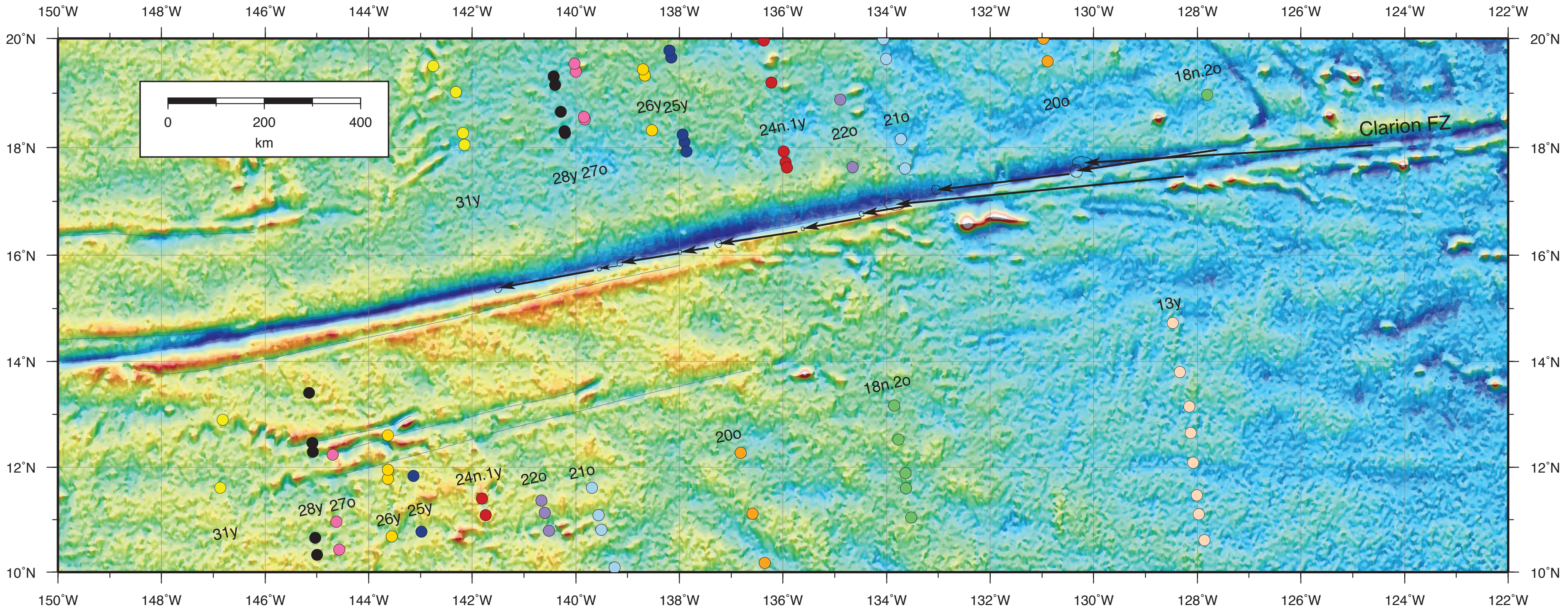

Figure DR7E: Clarion Fracture Zone

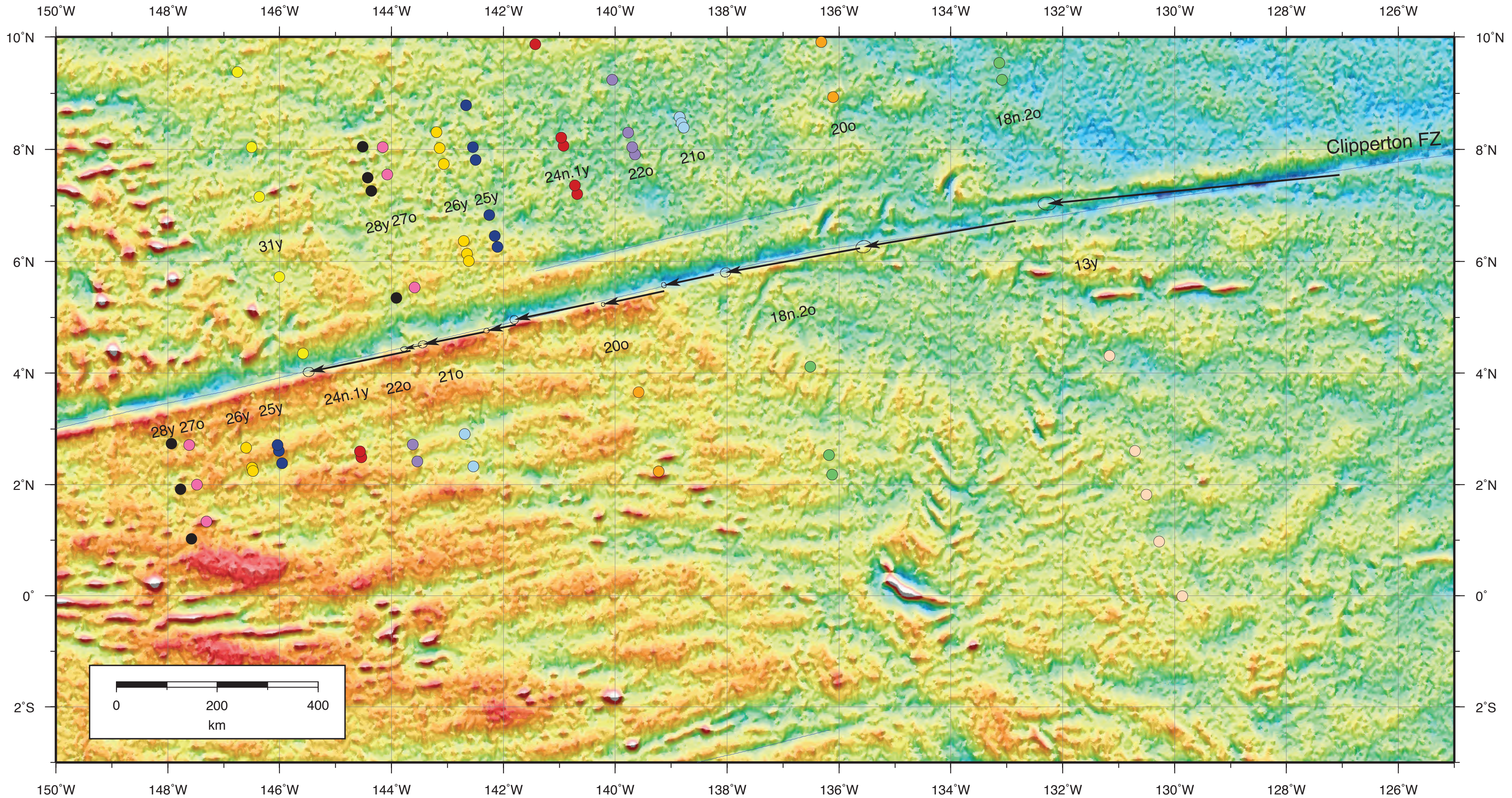

Figure DR7F: Clipperton Fracture Zone

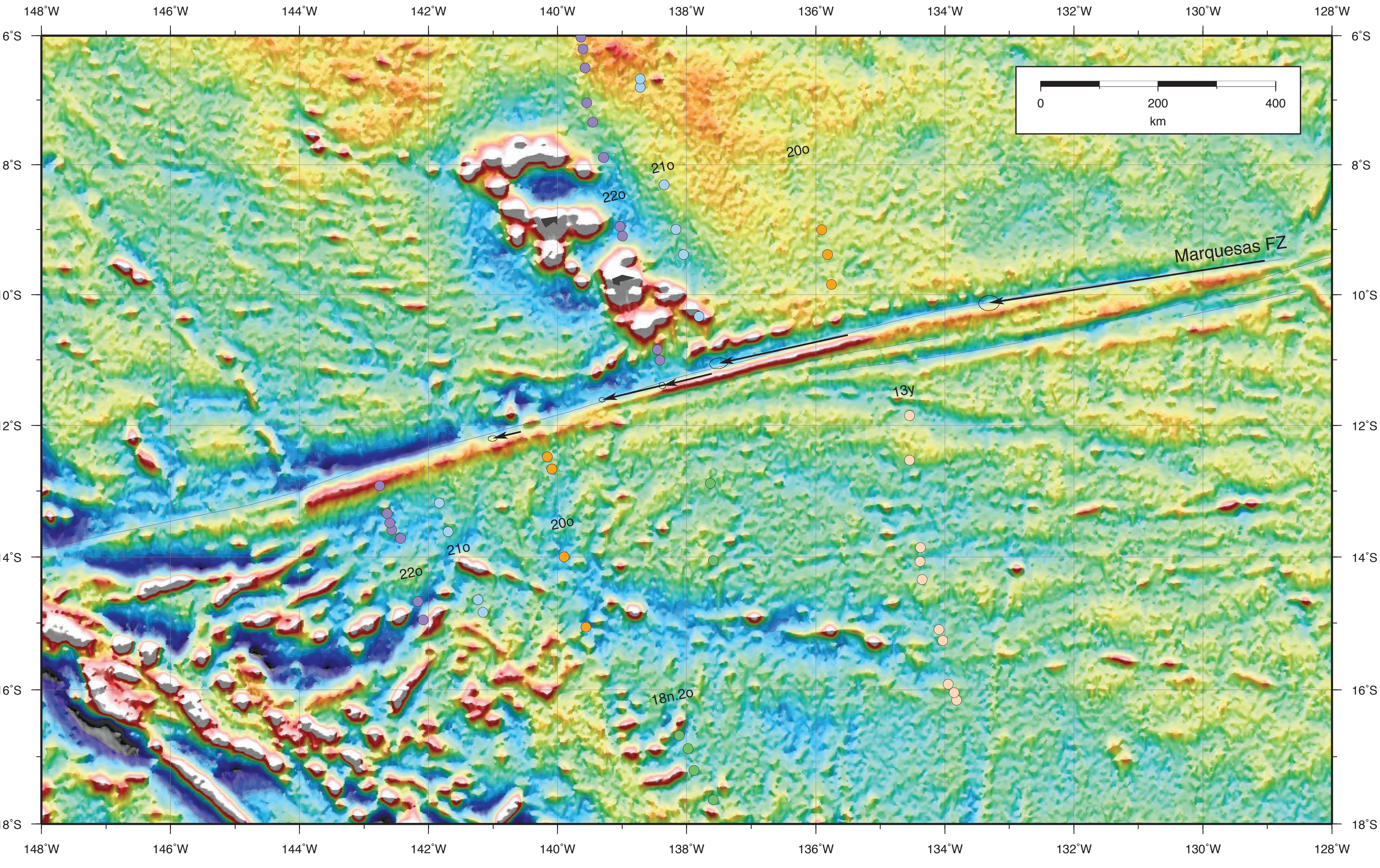

Figure DR7G: Marquesas Fracture Zone

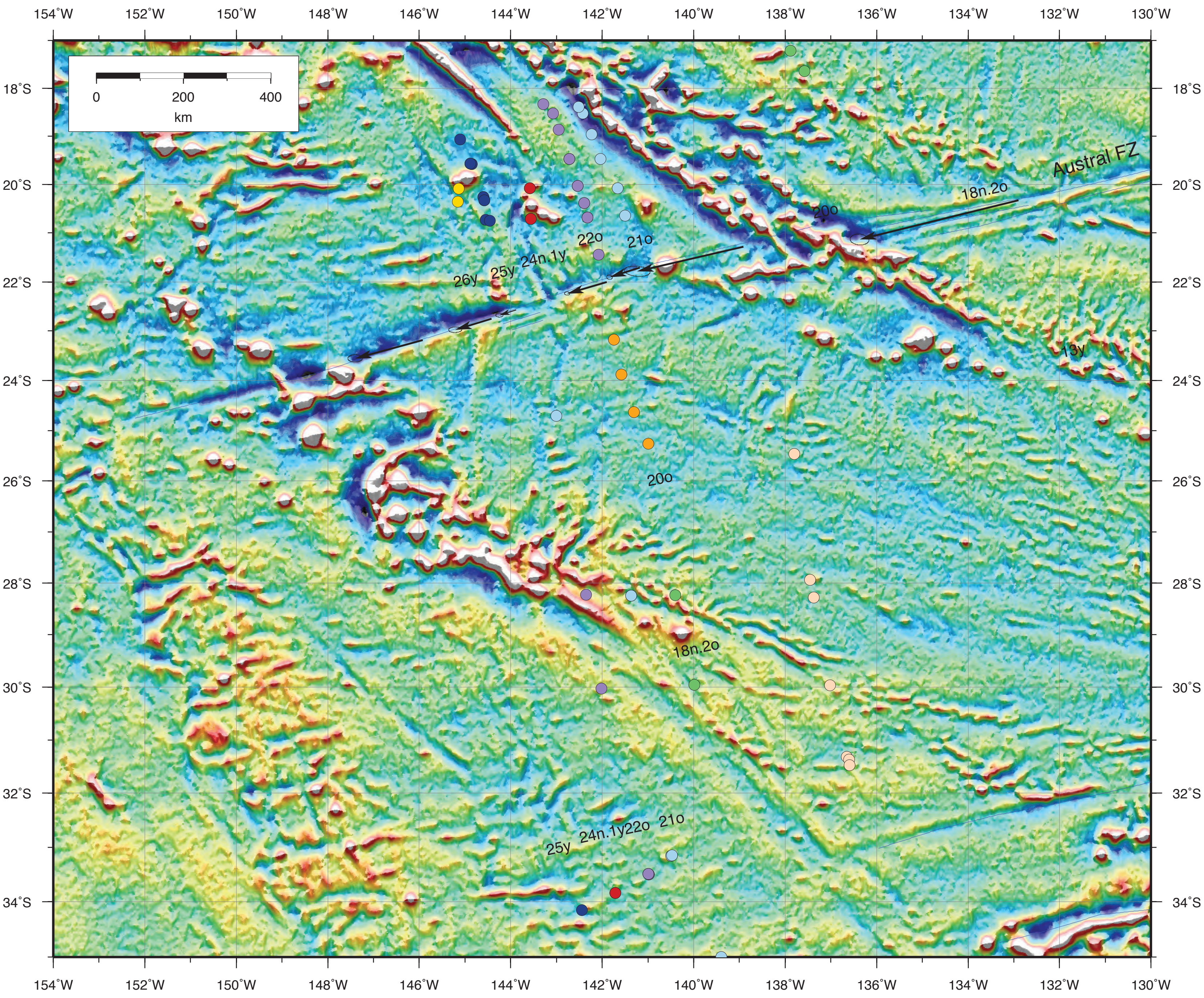

Figure DR7H: Austral Fracture Zone

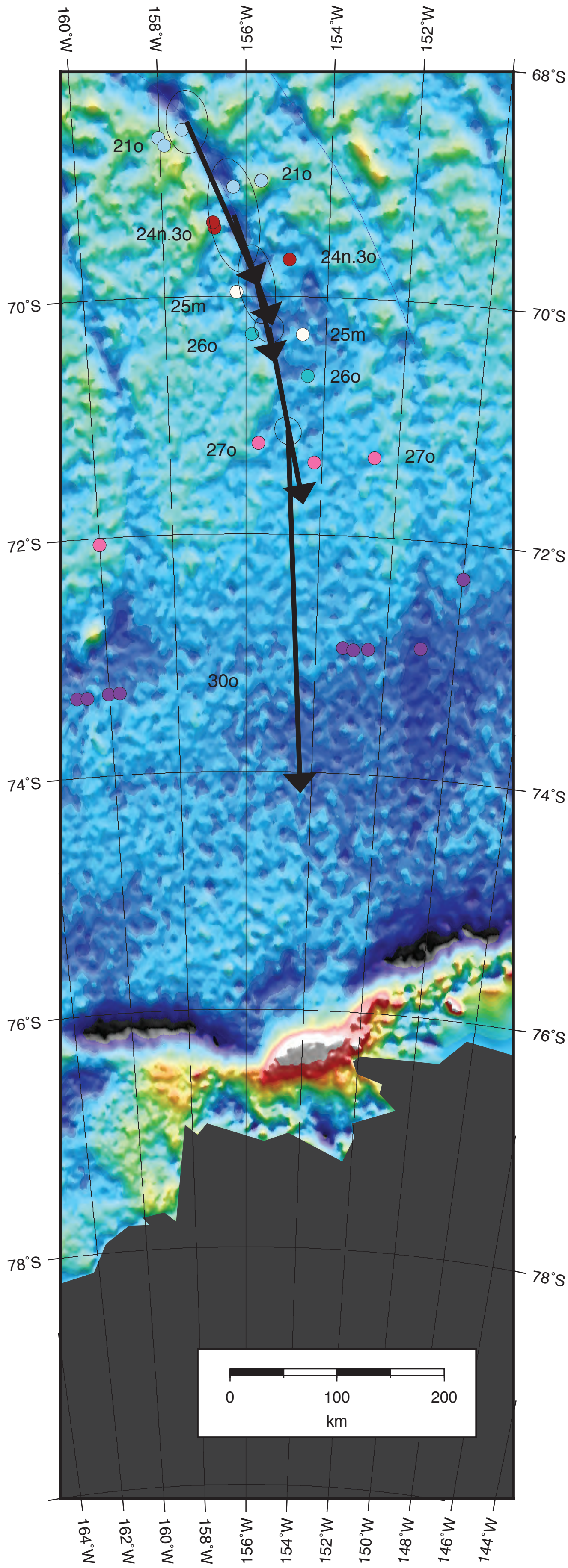

Figure DR8: Pitman Fracture Zone with velocity arrows and 95% uncertainties

References

Atwater, T. and Severinghaus, J., 1989. Tectonic maps of the northeast Pacific *in* Winterer, E. L., Hussong, D. M. and Decker, R. W., eds., The eastern Pacific Ocean and Hawaii, Geology of North America: Geological Society of America, Boulder, Colorado, v. N, p. 15-20.

Barckhausen, U., Bagge, M. and Wilson, D.S., 2013. Seafloor spreading anomalies and crustal ages of the Clarion-Clipperton Zone: Marine Geophysical Research, v. 34, p. 79-88, doi:10.1007/s11001-013-9184-6

Barckhausen, U., Ranero, C. R., Cande, S. C., Engels, M., and Weinrebe, W., 2008. Birth of an intraoceanic spreading center: Geology v. *36*, p.767-770.

Bird, P., 2003. An updated digital model of plate boundaries: Geochemistry, Geophysics, Geosystems, v. 4.

Boyden, J.A., Müller, R.D., Gurnis, M., Torsvik, T.H., Clark, J., Turner, M., Ivey-Law, H., Watson, R.J., and Cannon, J.S., 2011. Next-generation plate-tectonic reconstructions using GPlates, in: Geoinformatics: Cyberinfrastructure for the Solid Earth Sciences, edited by: Keller, G. R. and Baru, C., Chap. 7, Cambridge University Press, p. 95–116, doi:10.1017/CBO9780511976308.008,

Cande, S. C., and Kent, D. V., 1995. Revised calibration of the geomagnetic polarity timescale for the Late Cretaceous and Cenozoic: Journal of Geophysical Research: Solid Earth (1978–2012), v.100, p.6093-6095, doi:10.1029/94JB03098

Cande, S.C. and Haxby, W.F., 1991. Eocene propagating rifts in the southwest Pacific and their conjugate features on the Nazca plate: Journal of Geophysical Research: Solid Earth (1978–2012), vol. 96, p. 19609-19622, doi:10.1029/91JB01991

Cande, S.C., Raymond, C.A., Stock, J. and Haxby, W.F., 1995. Geophysics of the Pitman Fracture Zone and Pacific-Antarctic Plate: Science, v. 270, p. 947-953, doi:10.1126/science.270.5238.947

Caress, D.W., Menard, H. and Hey, R., 1988. Eocene reorganization of the Pacific-Farallon spreading center north of the Mendocino Fracture Zone: Journal of Geophysical Research: Solid Earth (1978–2012), vol. 93, p. 2813-2838, doi:10.1029/JB093iB04p02813

Chang, T., 1987. On the statistical properties of estimated rotations: Journal of Geophysical Research: Solid Earth (1978–2012), vol. 92, p. 6319-6329, doi:10.1029/JB092iB07p06319

Chang, T., 1988. Estimating the relative rotation of two tectonic plates from boundary crossings: Journal of the American Statistical Association, v. 83, p. 1178-1183, doi:10.1080/01621459.1988.10478717

Croon, M.B., Cande, S.C. and Stock, J.M., 2008. Revised Pacific-Antarctic plate motions and geophysics of the Menard Fracture Zone: Geochemistry, Geophysics, Geosystems, vol. 9, doi:10.1029/2008GC002019

Elvers, D., Peter, G., and Moses, R., 1967. Analysis of magnetic lineations in the North Pacific: Transactions of the American Geophysical Union, v. 48, p. 89.

Gaina, C., Müller, D. R., Royer, J. Y., Stock, J., Hardebeck, J., and Symonds, P., 1998. The tectonic history of the Tasman Sea: a puzzle with 13 pieces: Journal of Geophysical Research: Solid Earth (1978–2012), vol. 103, p. 12413-12433.

Gee, J.S. and Kent, D.V., 2007. Source of oceanic magnetic anomalies and the geomagnetic polarity time scale: Treatise on Geophysics, vol. 5: Geomagnetism: 455-507, doi:10.1016/B978-044452748-6.00097-3

Hellinger, S., 1981. The uncertainties of finite rotations in plate tectonics: Journal of Geophysical Research: Solid Earth (1978–2012), v. 86, p. 9312-9318, doi:10.1029/JB086iB10p09312

Kirkwood, B.H., Royer, J.Y., Chang, T.C. and Gordon, R.G., 1999. Statistical tools for estimating and combining finite rotations and their uncertainties: Geophysical Journal International, v. 137, p. 408-428, doi:10.1046/j.1365-246X.1999.00787.x

Matthews, K.J., Müller, R.D., Wessel, P. and Whittaker, J.M., 2011. The tectonic fabric of the ocean basins: Journal of Geophysical Research: Solid Earth (1978–2012), v. 116, doi:10.1029/2011JB008413

Müller, R.D., Sandwell, D.T., Tucholke, B.E., Sclater, J.G. and Shaw, P.R., 1991. Depth to basement and geoid expression of the Kane Fracture Zone: A comparison: Marine geophysical researches, v. 13, p. 105-129.

Munschy, M., Antoine, C. and Gachon, A., 1996. Evolution tectonique de la région des Tuamotu, océan Pacifique Central: Comptes rendus de l'Académie des sciences. Série 2. Sciences de la terre et des planètes, v. 323, p. 941-948.

Ogg, J.G. 2012. Geomagnetic Polarity Time Scale *in* Gradstein, F.M., Ogg, J.G, Schmitz, M., and Ogg, G., eds., The Geologic Time Scale 2012, Elsevier, doi: 10.1016/B978-0-444-59425-9.00005-6, 2012.

Rowan, C. J., and Rowley, D. B. 2014. Spreading behaviour of the Pacific-Farallon ridge system since 83 Ma: Geophysical Journal International, doi:10.1093/gji/ggu056

Royer, J.Y. and Chang, T., 1991. Evidence for relative motions between the Indian and Australian plates during the last 20 my from plate tectonic reconstructions: Implications for the deformation of the Indo-Australian plate: Journal of Geophysical Research: Solid Earth (1978–2012), v. 96, p. 11779-11802, doi:10.1029/91JB00897

Sandwell, D.T. and Smith, W.H., 2009. Global marine gravity from retracked Geosat and ERS-1 altimetry: Ridge segmentation versus spreading rate: Journal of Geophysical Research: Solid Earth (1978–2012), v. 114, doi:10.1029/2008JB006008

Seton, M., Whittaker, J.M., Wessel, P., Müller, R.D., DeMets, C., Merkouriev, S., Cande, S., Gaina, C., Eagles, G., Granot, R., Stock, J., Wright, N., Williams, S.E., 2014. Community infrastructure and repository for marine magnetic identifications: Geochemistry, Geophysics, Geosystems. doi:10.1002/2013GC005176

Vacquier, V., Raff, A.D. and Warren, R.E., 1961. Horizontal displacements in the floor of the northeastern Pacific Ocean: Geological Society of America Bulletin, v. 72, p. 1251-1258.

Wobbe, F., Gohl, K., Chambord, A. and Sutherland, R., 2012. Structure and breakup history of the rifted margin of West Antarctica in relation to Cretaceous separation from Zealandia and Bellingshausen plate motion: Geochemistry, Geophysics, Geosystems, v. 13, doi:10.1029/2011GC003742